Spectral-Energy Efficiency Tradeoff in Cognitive Satellite-Vehicular Networks Towards Beyond 5G

Yuhan Ruan*, Rui Zhang*, Yongzhao Li[*1], Cheng-Xiang Wang[†], and Hailin Zhang*

*State Key Laboratory of Integrated Service Network, Xidian University, Xi'an, 710071, China
[†]National Mobile Communications Research Laboratory, Southeast University, Nanjing, 210096, China
E-mail:{ryh911228@163.com, rui.zhang@stu.xidian.edu.cn, chxwang@seu.edu.cn, hlzhang@xidian.edu.cn}
[1]Corresponding author: yzhli@xidian.edu.cn

Abstract—**With the vigorous development of vehicular communications in 5G and beyond networks, cognitive satellite-terrestrial networks are expected to support multitudinous services and applications in future intelligent transportation systems and mobile Internet. To this aim, we introduce a cognitive satellite-vehicular network (CSVN) in this paper, where the secondary vehicular communications are featured with mobility. To realize friendly coexistence between satellite and vehicular networks as well as efficient resource utilization, we investigate the tradeoff between energy efficiency (EE) and spectrum efficiency (SE) and analyze the associated power allocation in the CSVN. Specifically, by introducing a preference factor which reflects the priority level of EE/SE, we firstly propose a unified EE-SE tradeoff metric to adapt to dynamic vehicular environments. Based on the formulated EE-SE tradeoff metric, we derive a power allocation strategy under the interference power constraints imposed by primary satellite communications. Finally, simulation results are provided to show the effects of preference factor, interference constraints, and vehicle velocity on the EE-SE tradeoff performance.**

Index Terms—**Cognitive satellite-vehicular networks, spectral efficiency, energy efficiency, power allocation, interference constraints.**

I. INTRODUCTION

With the increasing demand for applications and services in satellite communications as well as 5G and beyond communications, the available frequency resources have become scarce due to the dedicated frequency allocation of standardized wireless systems [1]. In this context, cognitive satellite-terrestrial networks (CSTNs), which enable spectrum sharing between satellite and terrestrial networks by employing cognitive radio (CR) technology, have emerged as one of the most promising infrastructures to alleviate the spectrum scarcity problem [2], [3]. On the other hand, with the development of intelligent transportation systems, vehicular communication is becoming a popular research topic both in industry and academia [4]. To keep pace with 5G and beyond communications and support satellite communications in mobile environments, e.g., emergency relief vehicles, satellite-vehicular communications have attracted increasing attentions [5], [6].

Inspired by the benefits of applying CR to satellite communications and the prospect of realizing vehicular communications in satellite-terrestrial networks, we introduce a cognitive satellite-vehicular network (CSVN) in this paper. Specifically, the satellite network is regarded as the primary system and the

terrestrial vehicular network operates as the secondary system. To realize friendly coexistence between satellite and vehicular networks, efficient resource allocation for the CSVN is a significant challenge due to the mobility feature of vehicular communications.

For conventional CSTNs, various resource allocation schemes were proposed to optimize the network performance [7]–[10]. Specifically, the authors in [7] proposed a carrier-power-bandwidth allocation scheme to maximize the satellite throughput. In [8], the authors conducted power allocation to maximize the achievable rate for CSTNs with amplify-and-forward relays. For real-time satellite applications in CSTNs, the authors in [9] conducted power control to maximize the delay-limited capacity without degrading the communication quality of the primary terrestrial user. Besides, beamforming based secure transmissions were studied in [10] to enhance the physical layer security for CSTNs. In these resource allocation schemes, transceivers in terrestrial networks are all assumed to be stationary. Whereas, for CSVNs, the high mobility of vehicular transceivers may have a significant influence on the propagation characteristics of wireless channel. As a result, resource allocation for CSVNs under a realistic mobile-to-mobile channel model needs to be further studied. Moreover, existing resource allocation schemes in CSTNs mainly concentrate on optimizing the network performance from the perspective of spectrum efficiency (SE), while ignoring the energy efficiency (EE), which is also a vital performance metric in the design of future environment-friendly satellite communications [11]. Thus, the consideration of both EE and SE is significant in 5G and beyond networks [12] [13].

To fill these gaps, we take both EE and SE into account in the CSVN. Considering EE and SE efficient transmission techniques are inconsistent with each other, we investigate the EE-SE tradeoff and the associated power allocation in the CSVN, where a three-dimensional (3D) vehicle-to-vehicle (V2V) channel model is adopted to characterize a realistic vehicular environment [14]. By analyzing the impact of vehicular density on EE and SE performance, we firstly propose an EE-SE tradeoff metric, where a preference factor is adopted to condense EE and SE into a single utility function to adapt to various vehicular scenarios. Based on the developed EE-SE tradeoff metric, we formulate the power allocation scheme as an optimization problem that minimizes the utility function of
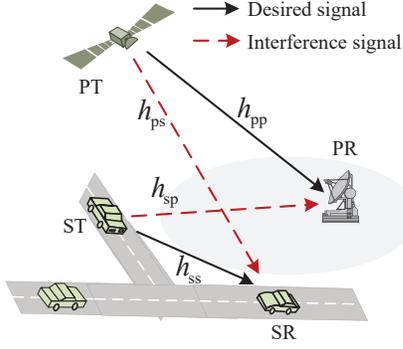
Fig. 1. System model of the underlay CSVN.

vehicular communications while guaranteeing the interference power constraints imposed by satellite communications. Then, employing the Charnes-Cooper transformation, we transform the fractional optimization problem into an equivalent convex problem and derive the optimal solution of the transmit power. Finally, simulation results are provided to evaluate the developed power allocation scheme and show the effects of preference factor, interference constraints, and vehicle velocity on the EE-SE tradeoff performance.

II. SYSTEM MODEL

As illustrated in Fig. 1, we consider a CSVN, where the satellite communication acts as the primary system and shares downlink spectral resource with the terrestrial V2V communication referred to as the secondary system in an underlay mode. In this case, the secondary vehicular transmitter (ST) will interfere the primary receiver (PR) while the secondary vehicular receiver (SR) will also suffer from the interference caused by the primary transmitter (PT). It is assumed that each node is equipped with a single antenna. We denote h_{ss}, h_{sp}, h_{ps}, and h_{pp} as the channel coefficients of ST→SR, ST→PR, PT→SR, and PT→PR links, respectively.

Given a system bandwidth W, the spectral efficiency (Ψ_{SE}, in bits/s/Hz) of V2V communications can be expressed as

$$\Psi_{SE} = \frac{\mathbb{E}\{C\}}{W} = \mathbb{E}\{\log_2(1+\gamma_s)\} \qquad (1)$$

where $\mathbb{E}\{\cdot\}$ denotes the expectation operator, C is the instantaneous capacity, and $\gamma_s = \frac{P_s|h_{ss}|^2}{N_0+P_p|h_{ps}|^2}$ is the received signal-to-interference-plus-noise ratio (SINR) at the vehicular receiver. Here, P_s and P_p are the transmit powers of the vehicular transmitter and the satellite, respectively, and N_0 is the average noise power.

Energy efficiency (Ψ_{EE}, in bits/Joule/Hz) is defined as the ratio of Ψ_{SE} to the total power expenditure (P_{tot}, in Watt) and can be formulated as

$$\Psi_{EE} = \frac{\Psi_{SE}}{\mathbb{E}\{P_{tot}\}} = \frac{\Psi_{SE}}{\mathbb{E}\{\eta P_s + P_0^C + P_0^S\}} \qquad (2)$$

where $1/\eta \in (0,1]$ denotes the drain efficiency of the power amplifier, P_0^C and P_0^S denote the circuit power and static

power, respectively. Since the circuit and static power consumptions are usually independent of data rate and can be regarded as constants for the transmitter, for notation simplicity, we use $P_{tot} = \eta P_s + P_0$ in the following, where $P_0 = P_0^C + P_0^S$.

In the following, we provide the related channel models involved in the CSVN.

A. V2V Channel Model

An accurate channel model is crucial for performance optimization of key 5G communication scenarios [15]. For the secondary V2V communication, we adopt the 3D V2V channel model proposed in [14] to accurately capture the effects of velocity and vehicular density on the channel characteristics. In this model, the radio propagation environment is characterized by 3D effective scattering with line-of-sight (LoS) and non-LoS (NLoS) components between the vehicular transmitter and receiver. Specifically, the NLoS components can be further classified as single bounced (SB) rays representing signals reflected only once during the propagation process and double bounced (DB) rays representing signals reflected more than once. For a given carrier frequency f, the channel coefficient h_{ss} can be expressed as

$$h_{ss} = h_{LoS} + \sum_{i=1}^{I} h_{SB_i} + h_{DB} \qquad (3)$$

where h_{LoS}, h_{SB_i}, and h_{DB} are the LoS component, SB component, and DB component, respectively. In this model, $I = 3$, which means there are three subcomponents for SB rays, i.e., SB_1 from the transmitter sphere, SB_2 from the receiver sphere, and SB_3 from the elliptic-cylinder. According to [14], we have

$$h_{LoS}(t) = \sqrt{\frac{K}{K+1}} e^{-j2\pi f\tau} e^{j2\pi f_s t \cos(\alpha_s^{LoS}-\lambda_s)\cos\beta_s^{LoS}}$$
$$\times e^{j2\pi f_d t \cos(\alpha_d^{LoS}-\lambda_d)\cos\beta_d^{LoS}} \qquad (4)$$

$$h_{SB_i}(t) = \sqrt{\frac{\eta_{SB_i}}{K+1}} \lim_{N_i\to\infty} \sum_{n_i=1}^{N_i} \frac{1}{\sqrt{N_i}} e^{j(\xi_{n_i}-2\pi f\tau_{n_i})}$$
$$\times e^{j2\pi f_s t \cos(\alpha_s^{(n_i)}-\lambda_s)\cos\beta_s^{(n_i)}} e^{j2\pi f_d t \cos(\alpha_d^{(n_i)}-\lambda_d)\cos\beta_d^{(n_i)}} \qquad (5)$$

$$h_{DB}(t) = \sqrt{\frac{\eta_{DB}}{K+1}} \lim_{N_1,N_2\to\infty} \sum_{n_1,n_2=1}^{N_1,N_2} \frac{1}{\sqrt{N_1,N_{2i}}}$$
$$\times e^{j(\xi_{n_1,n_2}-2\pi f\tau_{n_1,n_2})} e^{j2\pi f_s t \cos(\alpha_s^{(n_1)}-\lambda_s)\cos\beta_s^{(n_1)}}$$
$$\times e^{j2\pi f_d t \cos(\alpha_d^{(n_2)}-\lambda_d)\cos\beta_d^{(n_2)}} \qquad (6)$$

where $\alpha_s^{LoS} \approx \beta_s^{LoS} \approx \beta_d^{LoS} \approx 0$ and $\alpha_d^{LoS} \approx \pi$ with α_s^{LoS}, α_d^{LoS}, β_s^{LoS}, and β_d^{LoS} denoting azimuth angles of departure (AoD), azimuth angles of arrival (AoA), elevation AoD, and elevation AoA of the LoS component, respectively. Here, $\alpha_{s/d}^{(n_i)}$ and $\beta_{s/d}^{(n_i)}$ are the azimuth AoD/ azimuth AoA and elevation AoD/elevation AoA of the waves traveling from the effective scatterers $s^{(n_i)}$, respectively. Path delays for paths ST → SR, ST → $s^{(n_i)}$ → SR, and ST → $s^{(n_1)}$ → $s^{(n_2)}$ → SR are defined as τ, τ_{n_i}, and τ_{n_1,n_2}, respectively. We have K designates the Rician factor, indicating the power ratio of the LoS component to NLoS components. The ST and SR are assumed to be moving at the speed of $\nu_{s/d}$ in the direction

angle of $\lambda_{\text{s/d}}$, and f_{s} and f_{d} are the Doppler frequencies with respect to the ST and the SR, respectively. Parameters η_{SB_i} and η_{DB} specify the amount of power that SB and DB rays contribute to the total scattered power $1/(K+1)$, which satisfy $\sum_{i=1}^{I} \eta_{\text{SB}_i} + \eta_{\text{DB}} = 1$. Phases ξ_{n_i} and ξ_{n_1,n_2} are assumed to be independent and identically distributed random variables with uniform distributions over $[-\pi, \pi)$.

B. Generalized-K Channel Model

Apart from the V2V communication link, the considered network also involves in fixed-to-mobile/fixed links which consist of one terrestrial link (h_{sp}) and two land mobile satellite (LMS) links (h_{pp} and h_{ps}). In this paper, we model all fixed-to-mobile/fixed links uniformly as the generalized-K distribution because of its relatively simple mathematical form that allows an integrated performance analysis in composite multipath/shadowing fading environments. The generalized-K distribution is a mixture of Gamma-distributed shadowing and Nakagami-distributed multipath fading effect. According to [16], the generalized-K model can properly describe both the channel environments of satellite and terrestrial communications. For the generalized-K model, the probability density function (PDF) of $|h_i|^2$ ($i = \text{pp}, \text{ps}, \text{sp}$) can be written as

$$f_{|h_i|^2}(x) = \frac{2b_i^{\varphi_i + \varepsilon_i}}{\Gamma(\varepsilon_i)\Gamma(\varphi_i)} x^{\left(\frac{\varphi_i + \varepsilon_i}{2}\right) - 1} K_{\varphi_i - \varepsilon_i}\left(2b_i\sqrt{x}\right) \quad (7)$$

where $K_{\varphi_i - \varepsilon_i}(\cdot)$ is the modified Bessel function of the second kind with order $(\varphi_i - \varepsilon_i)$ and $b_i = \sqrt{\frac{\varphi_i \varepsilon_i}{\Omega_i}}$. Here, $\varepsilon_i \geq 0.5$ and $\varphi_i \geq 0$ are the multipath and shadowing parameters, respectively, Ω_i is the mean of the received local power.

III. POWER ALLOCATION FOR EE-SE TRADEOFF IN COGNITIVE SATELLITE-VEHICULAR NETWORKS

In this section, we investigate a power allocation strategy for the EE-SE tradeoff problem in CSVNs. According to the distinct performance characteristics in different vehicular traffic density (VTD) scenarios, a unified tradeoff metric is firstly developed to facilitate the applicability and tractability of resource management. Utilizing the EE-SE tradeoff metric, we propose an optimal power allocation scheme for vehicular communications to minimize the utility function under the interference power constraints imposed by satellite communications. Moreover, with the Charnes-Cooper transformation, the optimal solution for the transmit power is derived.

A. A Unified EE-SE Tradeoff Metric

In 5G and beyond communications, it is expected to maximize EE and SE simultaneously, which can be expressed as a multi-object optimization problem, i.e., $\max\{\Psi_{\text{SE}}, \Psi_{\text{EE}}\}$. Since EE and SE have different measurements and orders of magnitude, we normalize EE and SE with the maximum achievable EE value, i.e., $\Psi_{\text{MAX}}^{\text{EE}}$, and SE value, i.e., $\Psi_{\text{MAX}}^{\text{SE}}$, respectively. Noting that the maximum EE and SE are with respect to the transmit power. Here, instead of jointly maximizing $\frac{\Psi_{\text{SE}}}{\Psi_{\text{SE}}^{\text{MAX}}}$ and $\frac{\Psi_{\text{EE}}}{\Psi_{\text{EE}}^{\text{MAX}}}$, we minimize the inverse of the two objectives, i.e., $\min\left\{\frac{\Psi_{\text{SE}}^{\text{MAX}}}{\Psi_{\text{SE}}}, \frac{\Psi_{\text{EE}}^{\text{MAX}}}{\Psi_{\text{EE}}}\right\}$, to make SE
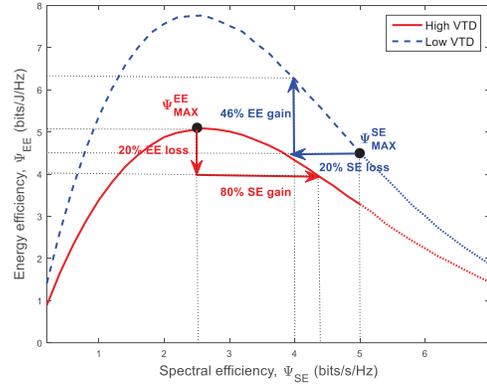

Fig. 2. EE versus SE in CSVNs with different VTD scenarios ($d_{\text{ss}} = 300$ m, $v = 10$ m/s, $P_0 = 150$ mW, $\bar{\gamma}_{\text{p}} = 8$ dB, $I_{\text{th}} = -90$ dBm).

as the common denominator and thus facilitate subsequent analysis [17].

Since we concentrate on investigating EE-SE tradeoff in CSVNs where vehicular communication is involved, it is necessary to analyze the impact of vehicular environment on the EE and SE performance at first. In vehicular communications, high VTD and low VTD scenarios are two typical scenarios corresponding to communication occurs in urban and rural areas, respectively. In a high VTD scenario with dozens of vehicles per square kilometer, the received power comes from all directions reflected by moving vehicles and DB rays dominate due to dense moving vehicles. In a low VTD scenario with less than ten vehicles per square kilometer, the received power comes mainly from specific directions identified by main stationary roadside scatterers and LoS component. As illustrated in [18], the VTD has a great impact on channel statistical properties, which eventually affect the performance of EE and SE.

To explicitly reveal the impact of VTD on EE and SE, we plot the achievable EE versus SE for V2V communications in different VTD scenarios in Fig. 2, where v is the velocity of V2V users, $\bar{\gamma}_{\text{p}} = P_{\text{p}}/N_0$ is the average interference-to-noise ratio (INR) from the satellite, and I_{th} is the interference threshold of satellite communications. Specific parameters of the high VTD and the low VTD used in the simulation can refer to [14]. As expected, the EE increases at the beginning and decreases afterwards in both scenarios, verifying the tradeoff between EE and SE. However, the slopes of two curves that EE versus SE are distinguishing. For example, for the low VTD scenario, a small degradation in EE (20%) around its peak value results in a significant gain in SE (80%). While for the high VTD scenario, we can achieve a considerable gain in EE (46%) with a small degradation in SE (20%). These observations illustrate that the high VTD scenario put more preference on SE than EE, while the low VTD scenario put more preference on EE than SE.

To make resource management applicable to various vehicular scenarios, we introduce a preference factor ω to condense EE and SE into a unified metric, which can be expressed as

$$\mathcal{F}(\omega, P_\mathrm{s}) = (1-\omega)\frac{\Psi_{\mathrm{MAX}}^{\mathrm{SE}}}{\Psi_{\mathrm{SE}}} + \omega\frac{\Psi_{\mathrm{MAX}}^{\mathrm{EE}}}{\Psi_{\mathrm{EE}}} \qquad (8)$$

where $\omega \in [0, 1]$ and $(1 - \omega)$ represent the importance weights of EE and SE, respectively. It can be seen that through the preference factor ω, the priority level of EE and SE can be flexibly adjusted to adapt to different VTD scenarios.

B. Power Allocation Based on EE-SE Tradeoff Metric

Based on the developed utility function, a power allocation scheme is then proposed for better coexistence of the vehicular and satellite communications. In the power allocation, we minimize the utility function of vehicular communications while restricting the interference power imposed at the satellite receiver below a predefined threshold, i.e., I_{th}. Thus, the optimization problem can be formulated as

$$\begin{array}{cl} \underset{P_\mathrm{s}(\omega, \gamma, h_{\mathrm{sp}}) \geq 0}{\text{minimize}} & \mathcal{F}(\omega, P_\mathrm{s}(\omega, \gamma, h_{\mathrm{sp}})) \\ \text{subject to} & P_\mathrm{s}(\omega, \gamma, h_{\mathrm{sp}})\,|h_{\mathrm{sp}}|^2 \leq I_{\mathrm{th}} \end{array} \qquad (9)$$

where $\gamma = \frac{|h_{\mathrm{ss}}|^2}{1+\bar{\gamma}_\mathrm{p}|h_{\mathrm{ps}}|^2}$. Since we consider the diverse preferences of different vehicular scenarios and interference constraints imposed by satellite communications, the transmit power of vehicular communications P_s is a function of ω, γ, and h_{sp}, i.e., $P_\mathrm{s}(\omega, \gamma, h_{\mathrm{sp}})$.

In the following, we first provide a solution for the optimization problem without the interference constraint, i.e.,

$$\underset{P_\mathrm{s}(\omega, \gamma) \geq 0}{\text{minimize}} \quad \frac{(1-\omega)\Psi_{\mathrm{MAX}}^{\mathrm{SE}} + \omega\Psi_{\mathrm{MAX}}^{\mathrm{EE}}\mathbb{E}_\gamma\{\eta P_\mathrm{s}(\omega, \gamma) + P_0\}}{\mathbb{E}_\gamma\{\log_2(1 + P_\mathrm{s}(\omega, \gamma)\gamma/N_0)\}}. \qquad (10)$$

By denoting $g(P_\mathrm{s}(\omega, \gamma))$ and $f(P_\mathrm{s}(\omega, \gamma))$ as the numerator and denominator, respectively, (10) can be equalized to

$$\underset{P_\mathrm{s}(\omega, \gamma) \geq 0}{\text{maximize}} \quad \frac{f(P_\mathrm{s}(\omega, \gamma))}{g(P_\mathrm{s}(\omega, \gamma))}. \qquad (11)$$

As observed, the objective function in (11) is a ratio of two functions with respect to $P_\mathrm{s}(\omega, \gamma)$. By applying Charnes-Cooper transformation $x = \frac{P_\mathrm{s}}{G(P_\mathrm{s})}$ and $t = \frac{1}{G(P_\mathrm{s})}$, the optimization problem in (11) can be reformulated as the following equivalent problem

$$\begin{array}{cl} \underset{P_\mathrm{s}(\omega, \gamma) \geq 0}{\text{maximize}} & t f\left(\frac{x}{t}\right) \\ \text{subject to} & t g\left(\frac{x}{t}\right) \leq 1. \end{array} \qquad (12)$$

Then, the optimization in (10) can be written as

$$\begin{array}{cl} \underset{P_\mathrm{s}(\omega, \gamma) \geq 0}{\text{maximize}} & t\mathbb{E}_\gamma\{\log_2(1 + P_\mathrm{s}(\omega, \gamma)\gamma/N_0)\} \\ \text{subject to} & t\left((1-\omega)\Psi_{\mathrm{MAX}}^{\mathrm{SE}} + \omega\Psi_{\mathrm{MAX}}^{\mathrm{EE}}\mathbb{E}_\gamma\{\eta P_\mathrm{s}(\omega, \gamma) + P_0\}\right) \leq 1. \end{array} \qquad (13)$$

In the following, we focus on settling the optimization problem (13). As the objective function in (13) is a logarithmic function with respect to $P_\mathrm{s}(\omega, \gamma,)$, thus it is concave. Besides, the constraint is an affine function and thus, the feasible set defined by constraint is a convex set. Thus, the Karush-Kuhn-Tucker (KKT) conditions are both sufficient and necessary for the optimality of (13). We employ the Lagrange multiplier method to obtain the optimal transmit power. Then, the partial Lagrangian of problem (13) is given by

$$\begin{aligned} \mathcal{L}(P_\mathrm{s}(\omega, \gamma), t, \ell) = {} & t\mathbb{E}_\gamma\{\log_2(1 + P_\mathrm{s}(\omega, \gamma)\gamma/N_0)\} \\ & + \ell\left(1 - t\left((1-\omega)\Psi_{\mathrm{MAX}}^{\mathrm{SE}} + \omega\Psi_{\mathrm{MAX}}^{\mathrm{EE}}\mathbb{E}_\gamma\{\eta P_\mathrm{s}(\omega, \gamma) + P_0\}\right)\right) \end{aligned} \qquad (14)$$

where $\ell > 0$ is the Lagrangian parameter. Then, the KKT condition $\frac{\partial \mathcal{L}(P_\mathrm{s}(\omega, \gamma), t, \ell)}{\partial P_\mathrm{s}(\omega, \gamma)} = 0$ can be written as

$$\frac{t\gamma}{\ln 2\,(P_\mathrm{s}(\omega, \gamma)\gamma + N_0)} - t\ell\omega\eta\Psi_{\mathrm{MAX}}^{\mathrm{EE}} = 0. \qquad (15)$$

Hence, the power allocation can be found as

$$P_\mathrm{s}' = \left[\frac{1}{\alpha\omega} - \frac{N_0}{\gamma}\right]^+ \qquad (16)$$

where $\alpha = \ln 2\ell\eta\Psi_{\mathrm{MAX}}^{\mathrm{EE}}$ and $[x]^+ = \max(0, x)$. The optimal value of ℓ can be found from the following equation

$$\begin{aligned} \mathbb{E}_\gamma\{\log_2(1 + P_\mathrm{s}'\gamma/N_0)\} - \ell\Big((1-\omega)\Psi_{\mathrm{MAX}}^{\mathrm{SE}} \\ + \omega\Psi_{\mathrm{MAX}}^{\mathrm{EE}}\left(\eta\mathbb{E}_\gamma\{P_\mathrm{s}'\} + P_0\right)\Big) = 0. \end{aligned} \qquad (17)$$

Note that (17) only depends on ℓ and is independent from t. The involved mean values can be derived as

$$\mathbb{E}_\gamma[P_\mathrm{s}'] = Q_1\frac{(\alpha\omega)^{-1}}{\tilde{\omega}^{\tilde{\varepsilon}_{\mathrm{ps}}}}G_{32}^{22}\left[\frac{(1+K)\tilde{\omega}}{b_{\mathrm{ps}}^2}\,\bigg|\,\begin{matrix}1 - \tilde{\varphi}_{\mathrm{ps}}, 1 + \tilde{\varphi}_{\mathrm{ps}}, 2 + \tilde{\varepsilon}_{\mathrm{ps}} \\ \tilde{\varepsilon}_{\mathrm{ps}}, 1 + p + \tilde{\varepsilon}_{\mathrm{ps}}\end{matrix}\right] \qquad (18)$$

$$\begin{aligned} \mathbb{E}_\gamma\left[\log_2\left(1 + \frac{P_\mathrm{s}'\gamma}{N_0}\right)\right] = {} & Q_1\sum_{l=0}^{L}\frac{(-1)^l\Gamma(l+1)}{l\tilde{\omega}^{\tilde{\varepsilon}_{\mathrm{ps}}}} \\ & \times G_{32}^{22}\left[\frac{(1+K)\tilde{\omega}}{b_{\mathrm{ps}}^2}\,\bigg|\,\begin{matrix}1 - \tilde{\varphi}_{\mathrm{ps}}, 1 + \tilde{\varphi}_{\mathrm{ps}}, 1 + \tilde{\varepsilon}_{\mathrm{ps}} \\ \tilde{\varepsilon}_{\mathrm{ps}} - l, 1 + p + \tilde{\varepsilon}_{\mathrm{ps}}\end{matrix}\right]. \end{aligned} \qquad (19)$$

Derivation can be found in Appendix A.

Assume that we have obtained the transmit power allocated for the interference unconstrained optimization. When the interference constraint is considered, the interference constraint in (9) can be equalized to a transmit power constraint, i.e., $P_\mathrm{s}(\omega, \gamma) \leq I_{\mathrm{th}}/|h_{\mathrm{sp}}|^2$. Following the similar discussion in [19], the optimal transmit power of (9) can be expressed as

$$P_\mathrm{s}^* = \min\left(\left[\frac{1}{\alpha\omega} - \frac{N_0}{\gamma}\right]^+, \frac{I_{\mathrm{th}}}{|h_{\mathrm{sp}}|^2}\right). \qquad (20)$$

C. The Effect of ω on the Optimal Transmit Power

From (20) we can see that the optimal transmit power P_s^* is dependent on the interference constraint (I_{th}), the channel gains $(|h_{\mathrm{ss}}|^2, |h_{\mathrm{sp}}|^2, |h_{\mathrm{ps}}|^2)$, and the preference factor ω, among which ω is the decisive parameter in terms of the tradeoff between EE and SE. In the following, we focus on discussing the impact of ω on P_s^*, where ω can be divided into three regions:

1) when $\omega < \frac{1}{\alpha}\left(\frac{N_0}{\gamma} + \frac{I_{\mathrm{th}}}{|h_{\mathrm{sp}}|^2}\right)^{-1}$, the ratio of EE in utility function is too small to affect the transmit power allocation. In this case, the power allocation scheme can be regarded as an optimization problem maximizing SE. Thus, the transmit power equals to the maximum value bounded by interference constraints, i.e., $P_\mathrm{s}^* = \frac{I_{\mathrm{th}}}{|h_{\mathrm{sp}}|^2}$.

2) when $\frac{1}{\alpha}\left(\frac{N_0}{\gamma} + \frac{I_{\mathrm{th}}}{|h_{\mathrm{sp}}|^2}\right)^{-1} \leq \omega \leq \frac{\gamma}{\alpha N_0}$, we have $P_\mathrm{s}^* = \frac{1}{\alpha\omega} - \frac{N_0}{\gamma}$. Thus, we should adjust the transmit power according to channel fading under the given preference factor ω.

3) when $\omega > \frac{\gamma}{\alpha N_0}$, we have $P_\mathrm{s}^* = 0$. Here, extremely poor link quality between vehicular users, such as serve
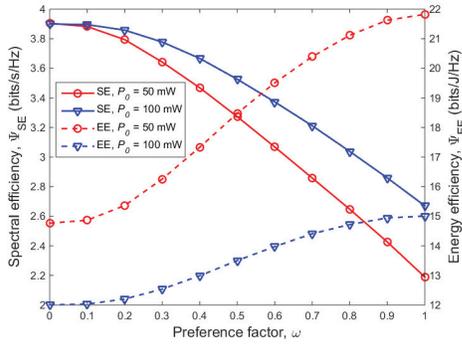
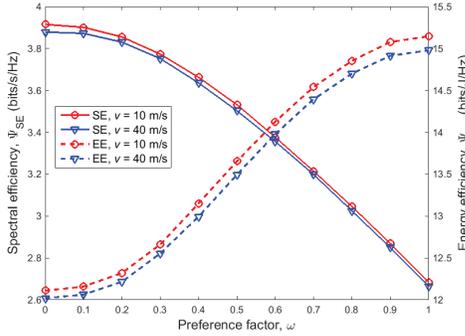Fig. 3. EE and SE versus preference factor ω for various P_0 in a low VTD scenario ($v = 5$ m/s, $I_{\mathrm{th}} = -95$ dBm).

Fig. 5. SE versus interference threshold I_{th} for various preference factors ω ($v = 5$ m/s, $P_0 = 100$ mW).

Fig. 4. EE and SE versus preference factor ω for various velocities v in a low VTD scenario ($P_0 = 100$ mW, $I_{\mathrm{th}} = -95$ dBm).

Fig. 6. EE versus interference threshold I_{th} for various preference factors ω ($v = 5$ m/s, $P_0 = 100$ mW).

fading, long distance, or serious interference from satellite, may result in vehicular communications being terminated. In this case, vehicular communications should employ flexible spectrum sharing method to avoid severer interference from primary satellite communications.

IV. RESULTS AND ANALYSIS

In this section, simulation results are provided to evaluate the developed power allocation scheme and show the effects of various parameters on the EE-SE tradeoff. In the simulations, we employ the path loss model $PL = 128.1 + 37.6\log_{10}(d\,[\text{in Km}])$ for terrestrial links and set $\eta = 1.2$, $N_0 = -114$ dBm, $d_{\mathrm{ss}} = 300$ m, $d_{\mathrm{sp}} = 500$ m, and the average INR from the satellite $\bar{\gamma}_{\mathrm{p}} = 5$ dB. For the generalized-K fading channels, the corresponding parameter φ_i can be linked to $\varphi_i = \frac{1}{e^{\sigma^2}-1}$, where σ is the standard deviation of the log-normal shadowing and increases as the amount of fading increases. We assume both h_{ps} and h_{sp} follow the the infrequent light shadowing (ILS) fading, where $\sigma_i = 0.115, \varepsilon_i = 3, \Omega_i = 1$ [16]. Besides, the 3D V2V channel parameters are the same as configured in Section IV in [14].

We firstly investigate the effects of the preference factor ω on the corresponding EE and SE. Taking low VTD scenario as an example, Fig. 3 presents the SE and EE versus the preference factor ω for various P_0 values. It can be seen that the SE decreases while the EE gradually increases with increasing ω. This can be explained by the fact that increasing
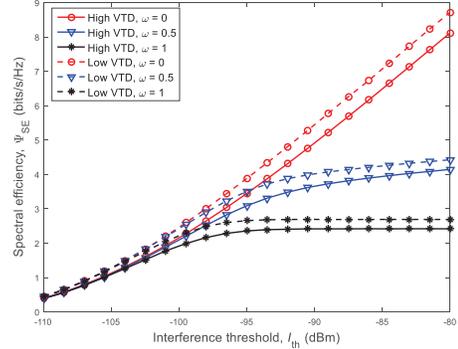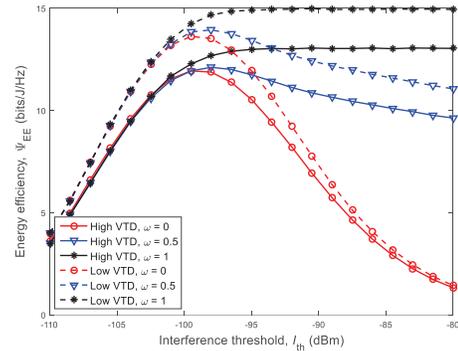
ω raises the importance of EE and diminishes the priority of SE, which coincide with our design intention. Especially, in the case of $\omega = 0$ and $\omega = 1$, the optimization reduces to the maximization of SE and EE, respectively. Moreover, different from EE, SE is independent of P_0. Thus, SE curves with various P_0 values overlap at the beginning while EE curves have different endpoints. It is interesting to note that when $\omega \in [0, 0.1]$, EE and SE almost remain constant. This is because in this region, the optimal transmit power is beyond the maximum allowable power bounded by interference constraints. Besides, as P_0 increases, we can achieve a higher SE while lower EE, which owing to the fact that the optimal transmit power would increase as P_0 gets larger. To illustrate the impact of V2V channel characteristics on system performance, we plot the SE and EE versus the preference factor ω for various vehicle velocities in Fig. 4. As observed, both the performance of SE and EE degrade as the velocity increases, revealing that a larger velocity represents a poor communication condition.

Fig. 5 and Fig. 6 depict SE and EE versus the interference threshold I_{th}. For both figures, communication occurring in high VTD scenario experiences a worse performance than that in low VTD scenario, either in terms of SE or EE. This is due to the fact that in high VTD scenario, the received power is reflected by dense moving vehicles, which result in a smaller Ricean factor. Moreover, In the case of $\omega = 0$ where the tradeoff optimization reduces to the SE maximization problem,

the optimal transmit power is exactly the maximum allowable power bounded by interference power constraints. Thus, as the interference constraint gets looser, i.e., I_{th} becomes larger, the optimal transmit power increases, resulting in a continuously growing in SE and simultaneously losing EE. When $\omega = 1$, the unified tradeoff optimization reduces to an EE maximization problem. In this case, from the figures we can observe that the maximum EE value can be achieved until I_{th} reaches to -95 dBm which corresponds to the transmit power P_{EE}^*. Therefore, when $I_{\text{th}} < -95$ dBm, SE and EE increase as I_{th} increases, while when $I_{\text{th}} > -95$ dBm, system always operates at the global optimal power P_{EE}^*. As a result, EE stabilizes at its maximum value and SE remains at $\Psi_{\text{SE}}(P_{\text{EE}}^*)$.

V. CONCLUSIONS

In this paper, we have investigated the EE-SE tradeoff and the associated power allocation in CSVNs. Firstly, we have proposed a unified EE-SE tradeoff metric with a preference factor, through which the priority level of EE/SE can be flexibly changed to adapt to dynamic surrounding circumstances. Moreover, the optimal transmit power has been derived under the interference constraints imposed by satellite communications. Furthermore, simulation results have demonstrated the viability of the unified EE-SE tradeoff metric.

ACKNOWLEDGMENT

APPENDIX A

From (16), $\mathbb{E}_\gamma\left[\log_2\left(1+\frac{P_s'\gamma}{N_0}\right)\right]$ ($\bar{\Psi}_{\text{SE}}$), can be written as

$$\bar{\Psi}_{\text{SE}} = \mathbb{E}_\gamma\left[\log_2\left(\frac{v}{\tilde{\omega}}\right)\right]\Big|_{\gamma \geq \tilde{\omega}} = \int_{\tilde{\omega}}^\infty \log_2\left(\frac{x}{\tilde{\omega}}\right)f_\gamma(x)\,dx. \quad (21)$$

where $\tilde{\omega} = \alpha\omega N_0$. To calculate (21), we need to derive $f_\gamma(x)$ firstly. From $\gamma = \frac{|h_{\text{ss}}|^2}{1+\bar{\gamma}_p|h_{\text{pd}}|^2}$, $f_\gamma(x)$ can be written as

$$f_\gamma(x) = \int_0^\infty (y+1)\,f_{\bar{\gamma}_p|h_{\text{ps}}|^2}(y)\,f_{|h_{\text{ss}}|^2}(x(y+1))\,dy. \quad (22)$$

By substituting (7) and the PDF shown in [19, Eq. (5)] into (22), and expanding the series expression for $I_0(x)$ [20, Eq. (8.447.1)], $f_\gamma(x)$ can be expressed as

$$f_\gamma(x) = \frac{2b_{\text{ps}}^{\varphi_{\text{ps}}+\varepsilon_{\text{ps}}}(1+K)e^{-K}}{\Gamma(\varphi_{\text{ps}})\Gamma(\varepsilon_{\text{ps}})(\bar{\gamma}_p)^{\tilde{\varepsilon}_{\text{ps}}}}\sum_{p=0}^L\frac{K^p(1+K)^p}{(p!)^2}x^p$$
$$\times \int_0^\infty y^{p+\tilde{\varepsilon}_{\text{ps}}}e^{-(1+K)xy}K_{\varphi_{\text{ps}}-\varepsilon_{\text{ps}}}(2b_{\text{ps}}\sqrt{y})\,dy \quad (23)$$

where $\tilde{\varepsilon}_{\text{ps}} = \frac{\varphi_{\text{ps}}+\varepsilon_{\text{ps}}}{2}$. In the above derivation, we assume that the interference dominates the noise [13]. By expressing $K_{\varphi_{\text{ps}}-\varepsilon_{\text{ps}}}(2b_{\text{ps}}\sqrt{y})$ in terms of Meijer-j function and using [20, Eq. (7.813.1), (9.31.2)], $f_\gamma(x)$ can be obtained as

$$f_\gamma(x) = Q_1 x^{-\tilde{\varepsilon}_{\text{ps}}-1}G_{21}^{12}\left[\frac{(1+K)}{b_{\text{ps}}^2}x\;\middle|\;\begin{matrix}1-\tilde{\varphi}_{\text{ps}},1+\tilde{\varphi}_{\text{ps}}\\1+p+\tilde{\varepsilon}_{\text{ps}}\end{matrix}\right] \quad (24)$$

with $Q_1 = \frac{b_{\text{ps}}^{\varphi_{\text{ps}}+\varepsilon_{\text{ps}}}e^{-K}}{\Gamma(\varphi_{\text{ps}})\Gamma(\varepsilon_{\text{ps}})\bar{\gamma}_p^{\tilde{\varepsilon}_{\text{ps}}}}\sum_{p=0}^L\frac{K^p(1+K)^{-\tilde{\varepsilon}_{\text{ps}}}}{(p!)^2}$, $\tilde{\varphi}_{\text{ps}} = \frac{\varphi_{\text{ps}}-\varepsilon_{\text{ps}}}{2}$.

Then, by substituting $f_\gamma(x)$ in (24) into (21), expanding the log function into the sum of L series, and utilizing [20, Eq. (7.811.3)], the analytical expression of $\bar{\Psi}_{\text{SE}}$ can be finally derived as shown in (19). With the similar derivation steps of $\bar{\Psi}_{\text{SE}}$, $\mathbb{E}_\gamma[P_s']$ can be calculated as shown in (18).

REFERENCES

[1] Y. Ruan, Y. Li, C.-X. Wang, R. Zhang, and H. Zhang, "Performance evaluation for underlay cognitive satellite-terrestrial cooperative networks", *Sci. China Inf. Sci.*, vol. 61, pp. 1–11, Oct. 2018.

[2] M. Jia, X. Gu, Q. Guo, W. Xiang, and N. Zhang, "Broadband hybrid satellite-terrestrial communication systems based on cognitive radio toward 5G," *IEEE Wireless Commun.*, vol. 23, no. 6, pp. 96–106, Dec. 2016.

[3] Y. Ruan, Y. Li, C-X. Wang, R. Zhang, and H. Zhang, "Effective capacity analysis for underlay cognitive satellite-terrestrial networks," in *Proc. IEEE ICC'17*, Paris, France, May 2017, pp. 1–6.

[4] S. A. A. Shah *et al.*, "5G for vehicular communications," *IEEE Commun. Mag.*, vol. 56, no. 1, pp. 111–117, Jan. 2018.

[5] T. M. Nguyen, A. T. Guillen, and S. S. Matsunaga, "Practical achievable capacity for advanced SATCOM on-the-move," in *Proc. IEEE MIL-COM'16*, Baltimore, USA, Nov. 2016, pp. 150–155.

[6] G. Cocco, N. Alagha, and C. Ibars, "Cooperative coverage extension in vehicular land mobile satellite networks," *IEEE Trans. Veh. Technol.*, vol. 65, no. 8, pp. 5995–6009, Aug. 2016.

[7] E. Lagunas *et al.*, "Resource allocation for cognitive satellite communications with incumbent terrestrial networks," *IEEE Trans. Cognitive Commun. Networking*, vol. 1, no. 3, pp. 305–317, Sep. 2015.

[8] Z. Li, F. Xiao, S. Wang, T. Pei, and J. Li, "Achievable rate maximization for cognitive hybrid satellite-terrestrial networks with AF-relays," *IEEE J. Sel. Areas Commun.*, vol. 36, no. 2, pp. 304–313, Feb. 2018.

[9] S. Shi, G. Li, K. An, Z. Li, and G. Zheng, "Optimal power control for real-time applications in cognitive satellite terrestrial networks," *IEEE Commun. Lett.*, vol. 21, no. 8, pp. 1815–1818, July 2018.

[10] J. D *et al.*, "Secure satellite-terrestrial transmission over incumbent terrestrial networks via cooperative beamforming," *IEEE J. Sel. Areas Commun.*, vol. 36, no. 7, pp. 1367–1382, July 2018.

[11] F. Alagoz and G. Gur, "Energy efficiency and satellite networking: a holistic overview," *IEEE Proc.*, vol. 99, no. 11, pp. 1954–1979, Nov. 2011.

[12] C.-X. Wang *et al.*, "Cellular architecture and key technologies for 5G wireless communication networks," *IEEE Commun. Mag.*, vol. 52, no. 2, pp. 122–130, Feb. 2014.

[13] Y. Ruan, Y. Li, C.-X. Wang, and R. Zhang, "Energy efficient adaptive transmissions in integrated satellite-terrestrial networks with SER constraints," *IEEE Trans. Wireless Commun.*, vol. 17, no. 1, pp. 210–222, Jan. 2018.

[14] Y. Yuan *et al.*, "Novel 3D geometry-based stochastic models for non-isotropic MIMO vehicle-to-vehicle channels," *IEEE Trans. Wireless Commun.*, vol. 13, no. 1, pp. 298–309, Jan. 2014.

[15] S. Wu, C.-X. Wang, H. Aggoune, M. M. Alwakeel, and X. You, "A general 3D non-stationary 5G wireless channel model," *IEEE Trans. Commun.*, vol. 66, no. 7, pp. 3065–3078, July 2018.

[16] K. P. Peppas, "Accurate closed-form approximations to generalised-K sum distributions and applications in the performance analysis of equal-gain combining receivers," *IET Commun.*, vol. 5, no. 7, pp. 982–989, May 2011.

[17] W. Yu, L. Musavian, and Q. Ni, "Tradeoff analysis and joint optimization of link-layer energy efficiency and effective capacity toward green communications," *IEEE Trans. Wireless Commun.*, vol. 15, no. 5, pp. 3339–3353, May 2016.

[18] R. Zhang, Y. Li, C.-X. Wang, Y. Ruan, and H. Zhang, "Energy efficient power allocation for mobile D2D communications with peak/average interference constraints," *Sci. China Inf. Sci.*, vol. 61, pp. 1–3, Aug. 2018.

[19] R. Zhang *et al.*, "Energy-spectral efficiency trade-off in underlaying mobile D2D communications: an economic efficiency perspective," *IEEE Trans. Wireless Commun.*, vol. 17, no. 7, pp. 4288–4301, July 2018.

[20] I. S. Gradshteyn and I. M. Ryzhik, *Table of Integrals, Series, and Products*, 6th ed. Academic Press, 2000.